Understanding How Metal-Ligand Coordination Enables Solvent Free Ionic Conductivity in PDMS

Xinyue Zhang,[†,¶] Jinyue Dai,[‡,¶] Max Tepermeister,[‡] Jingjie Yeo,[‡] and Meredith N. Silberstein[*,‡]

†*Department of Materials Science and Engineering, Cornell University, Ithaca, NY 14850, USA*

‡*Sibley School of Mechanical and Aerospace Engineering, Cornell University, Ithaca, NY 14853, USA*

¶*Authors contributed equally to this work.*

E-mail: meredith.silberstein@cornell.edu

Abstract

Ionically conductive polymers are commonly made of monomers containing high polarity moieties to promote high ion dissociation, like poly(ethylene oxide) (PEO), polyvinylidene difluoride (PVDF), poly(vinyl alcohol) (PVA). However, the glass transition temperature (T_g) of these polymers are relatively high, and therefore yields a glassy state at room temperature and limits the mechanical flexibility of the material. Although polydimethylsiloxane (PDMS) has many attractive physical and chemical properties, including low glass transition temperature, mechanical flexibility, and good biocompatibility, its low dielectric constant suppresses ion dissociation. In this paper, we overcome this shortage by functionalizing the PDMS with ligands that can form labile coordination with metal ions, which greatly promotes the ion dissociation and improves the ionic conductivity by orders of magnitude. By combining an experimental study with a fully atomistic molecular dynamics simulation, we systematically

investigated the ion transport mechanisms in this low T_g, low intrinsic conductivity material.

Introduction

Ionically conductive polymers, also named polymer electrolytes, are emerging as popular material candidates for enabling cutting-edge technologies including energy storage, soft robotics, biomedical devices, and bioinspired sensory systems.[1–5] In recent decades, liquid, gel, and solid-state ionically conductive polymers have been developed to fulfill various needs. For example, most of the pioneering studies on polymer electrolytes are based on polyethylene oxide (PEO) complexed with alkali metal salts.[6,7] Ionic liquids have been either mixed into neutral polymer bases or polymerized into poly(ionic liquid)s (PILs) for engineering various electrochemical devices.[8,9] Ionic polymer metal composites (IPMC) consisting of a polyelectrolyte membrane placed in between two noble metal electrodes have been studied to enable large actuation under an applied electric field.[10] Continued effort has been made to both develop novel ionically conductive polymers and understand fundamental ion conducting mechanisms to enable rational design based on application functional requirements.

Ion mobility and ion concentration are the two key factors governing ionic conductivity of a polymer; the former is not only directly related to the identity and quantity of cations and anions, but is also greatly affected by the physical and chemical characteristics of the polymer matrix bearing the ions.[11] Polymers with low glass transition temperature and low crystallinity are good candidates to achieve high ionic conductivity at room temperature for practical applications.[12] However, polyelectrolytes are predominantly made of polymers containing high polarity backbones to facilitate ion dissociation, which raise the glass transition temperature or promote crystallinity by increasing intermolecular interactions.[13] In contrast, polymers with low dielectric constants, like PDMS, have low glass transition temperatures and maintain an amorphous state, but are barely ionically conductive without modification

due to poor salt dissociation.[14] Metal-ligand coordination as a non-covalent interaction has been extensively applied in polymer matrices to enhance the mechanical toughness, tune viscoelasticity, and enable self-healing.[15–20] In recent years, metal-ligand coordination has also been studied as a means of designing ionically conductive polymers.[21–24] For example, imidazole-and imidazolium-containing polymers which can bind with metals have been synthesized and studied.[25,26] This moiety is particularly interesting due to its wide prevalence in nature and in the human body, and therefore relevance in bioactive applications.[25] In addition, polymer electrolytes containing metal-ligand coordination such as Li^+ coordinated poly(N-methyl-malonic amide) and Zn^{2+} coordinated polyacrylamide have been developed for all-solid-state batteries.[27,28]

It is vital to build fundamental understanding of the ion conducting mechanisms of these amorphous, elastomeric, metal-coordinated polymers, and the relation of these mechanisms to the polymer structure. Molecular dynamics (MD) simulations are a powerful approach to provide detailed insights into transport phenomenon in ionic polymeric materials at the atomistic level.[29,30] So far, MD simulations related to ionic conductivity have mainly focused on collecting single ion dynamics. Ionic conductivity is commonly determined with the Nernst-Einstein (NE) equation, which gives the conductivity as directly proportional to the diffusion coefficients of the ions. The NE approximation works rather well for dilute systems with high dielectric constants, but fails in the concentrated ion regime.[31,32] An alternative approach by Wheeler and Newman following a Green-Kubo methodology in the Stephan-Maxwell framework reported large noise determining off-diagonal transport coefficients.[33] Grossman et al. proposed the cluster Nernst Einstein (cNE) method that accounts for salt nucleation.[34] They showed that their method could reproduce the experimental results of PEO-based electrolytes at high salt loading.[34] Their method should be also applicable to other cases with solvent-free or low dielectric constant, where the capacity to dissociate ion pairs is too weak and therefore the ions form clusters.

In this study, we combine in-depth experimental studies with fully atomistic MD simu-

lations to unveil ion conducting mechanisms in metal-coordinated PDMS. A low molecular weight polydimethylsiloxane (PDMS) end-functionalized with pyridyl imine ligands is selected as the model system, and a series of Li and Cu salts are added to form polymer complexes. Factors that govern the ionic conductivity of the material, including ion dissociation, ion concentration, and chain mobility, are discussed in the context of the metal-ligand coordination density and strength. Firstly, we highlight that the formation of metal-ligand coordination promotes salt dissociation into ions and therefore enhances the ionic conductivity of the PDMS complex as compared to the direct mixing of pristine PDMS and metal salt. Next, we show that the choice of counter anion, metal cation, and ion concentration can vary the ionic conductivity of PDMS by orders of magnitude due to the distinct cation-anion interactions. To elucidate the ion transport mechanisms, a range of properties are computed from the MD simulations, including the ion and polymer chain diffusion coefficients, ionic conductivity, and cluster analysis. Furthermore, based on our observations of the single metal cation coordinated PDMS, we propose and prove that a synergistic effect on the mechanical strength and ionic conductivity of the PDMS would be achieved by coordinating with two metal cation species: the majority component is the metal cation with weak coordination, that is primarily responsible for the ion conductivity; whereas the minority component is the metal cation with strong coordination that enhances the mechanical strength of the network. This paper provides insights into strategic design of ionically conducting polymers that would benefit a range of applications.

Results and Discussions

The effect of metal-ligand coordination

To understand how metal-ligand coordination promotes the ionic conductivity of a polymer, we choose low molecular weight PDMS as the polymer precursor because of its many advantageous features. First, PDMS has a low glass transition temperature ($T_g \approx -123\,^{\circ}\mathrm{C}$), yielding

dynamic chain motion at room temperature, which facilitates the transport of ions.[35,36] Second, PDMS has low inherent ion impurity content and low dielectric constant ($\kappa \approx 2.3-2.8$), which serves as a non-conductive baseline and creates a clear contrast in the ionic conductivity of the polymer before and after introducing metal-ligand coordination.[37,38] Furthermore, ion interaction in the system is mainly mediated by the metal-ligand coordination rather than the solvation of polymer backbone, which offers us a good model to decouple the effect of metal-ligand coordination from other factors that contribute to the ionic conductivity.[14,39] Third, PDMS has many good physical and chemical properties such as being stretchable and inert. Finally, PDMS is easy to fabricate and low cost, which makes it a popular material candidate for next-generation ionic devices.[5,40]

We create a model system by functionalizing the ends of low molecular weight PDMS with a metal coordinating ligand. Pyridyl imine is selected as the functional group because it is a versatile ligand that can coordinate with various metal cations.[41] The model system (**PDMS-L**, L represents ligand functionalization) is synthesized via a condensation reaction between aminopropyl terminated PDMS and 2-pyridinecarboxaldehyde according to a previously reported procedure, yielding a yellow oil-like product (Figure 3a).[42] The structure of **PDMS-L** is confirmed by ^{1}H NMR (Figure S1). Based on the ratio of the hydrogen atoms in the dimethylsiloxane backbone to the hydrogen atoms in the pyridyl imine end groups, which is calculated from the integration of different peak area in the ^{1}H NMR spectrum, the number average molecular weight (M_n) of **PDMS-L** is around 2000 g/mol.

To study how the formation of coordination complexes affects the ionic conductivity of the model system, a monovalent metal cation Li^+ is added first. Since Li^+ has a coordination number of $4-6$ with different ligand molecules, it is important to determine the coordination stoichiometry between Li^+ and the pyridiyl imine ligand.[43,44] Therefore, a small-molecule model ligand, N-propyl(2-pyridyl)methanimine, is synthesized (Figure S2), and is combined with lithium trifluoromethanesulfonate (LiOTf) salt to form a small-molecule Li^+-pyridyl imine complex. This complex is analyzed by mass spectrometry (MS) in electrospray ioniza-

tion (ESI) positive ion mode, and the molecular weight is found to be 453.18 *Da*, indicating that the ratio between Li^+ and pyridyl imine ligand is 1 : 2 (Figure S3). Since pyridyl imine groups are present at the both ends of the PDMS chain, this number implies that the ligands are fully coordinated with Li^+ when the molar ratio of PDMS to LiOTf is 1 : 1.

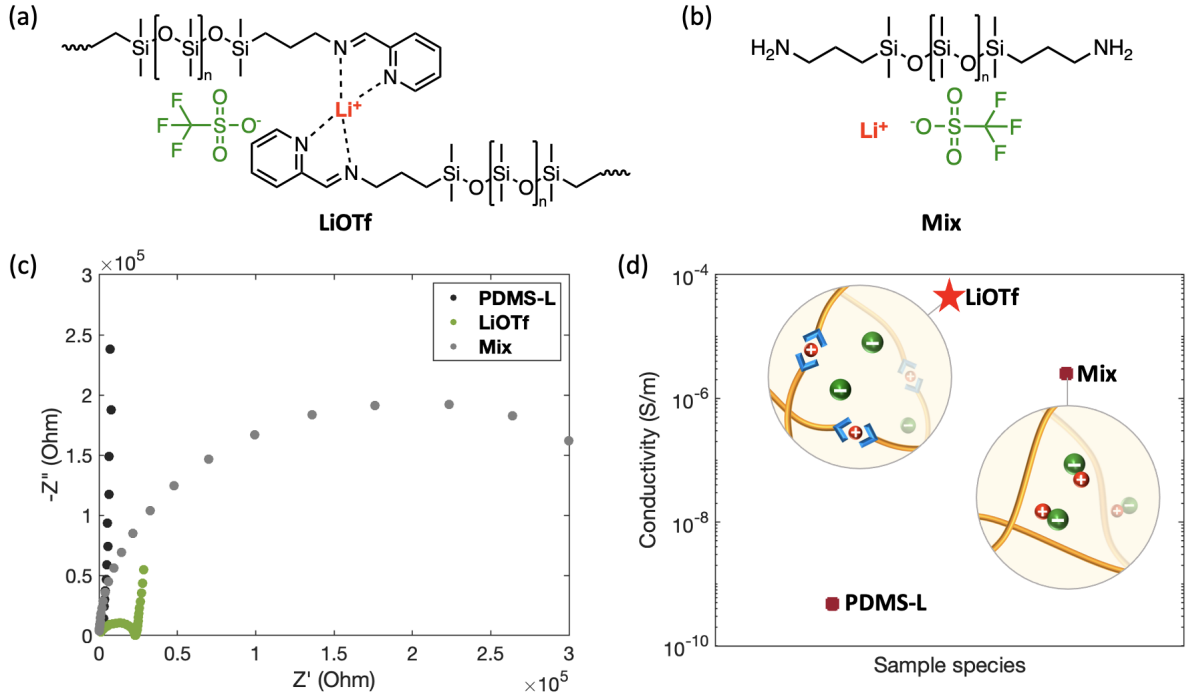

Figure 1: Comparison between the model and control systems. The chemical structure of (a) the LiOTf coordinated PDMS, **LiOTf**. (b) the mixture of pristine PDMS and LiOTf, **Mix**. (c) Nyquist plots of the model and control systems measured by EIS. (d) Comparison of ionic conductivity of the model and control systems. Schematics showing different degree of cation-anion dissociation in the PDMS with and without ligand functionalization.

Next, PDMS with this 1 : 1 molar PDMS-L to LiOTf ratio is synthesized (**LiOTf**, Figure 1a). Two additional polymers are synthesized as controls: (1) **PDMS-L** with no LiOTf salt, and (2) pristine PDMS (not ligand functionalized) mixed with same quantity of LiOTf salt (**Mix**, Figure 1b). It is worth highlighting that additional solvent is not necessary to facilitate the mixing of the PDMS and LiOTf salt in the preparation of **LiOTf** and **Mix**, because LiOTf salt can slowly but completely dissolve in the PDMS under vigorous stirring. This is in contrast to the conventional preparation procedure, which uses solvent casting followed by solvent evaporation to prepare dry polymer electrolytes.[45] Given that

organic solvents are hard to completely remove even after careful vacuum drying, causing variation in the measurement of ionic conductivity, we think it is advantageous that this model system does not require extra solvents to synthesize Li^+ coordinated samples.[11] The formation of a complex between the PDMS and Li^+ is verified by Fourier-transform infrared spectroscopy (FTIR) (Figure S5). The IR spectra of the samples are normalized by the intensity of the peak at 1259 cm^{-1}, corresponding to CH_3 symmetric bending in Si-CH_3 on the PDMS backbone.[46] Compared to the spectrum of **PDMS-L**, in **LiOTf** the absorbance intensity at the wavenumber 1650 cm^{-1} decreases and a new peak rises at a lower wavenumber 1593 cm^{-1}. This peak shift results from the decreased bond order of C=N stretching in the coordinated pyridyl imine ligands.[47] The presence of OTf^- anions is confirmed by the new peaks between the wavenumber of 1230 cm^{-1} and 1300 cm^{-1} from the overlapped C-F and S=O stretching.[48]

We then compare the ionic conductivity of the model and the controls using electrochemical impedance spectroscopy (EIS), which shows distinct results in Nyquist plots (Figure 1c). **PDMS-L** has an extremely low ionic conductivity that is below the limit of detection because of the low ion impurity content ($\sigma < 4.8 \times 10^{-10}\ S/m$). In contrast, the ionic conductivity of **LiOTf** increases by 5 orders of magnitude, yielding the value of $(4.28 \pm 0.22) \times 10^{-5}\ S/m$. Although **Mix** also shows improved ionic conductivity ($\sigma = (2.51 \pm 0.12) \times 10^{-6}\ S/m$) compared to the pure PDMS, it is only about 6% of the value of **LiOTf**. Since the same amount of LiOTf salt is added into the PDMS with and without ligand functionalization, the extent of salt ionization determines the ionic conductivity of the material.[39] The significantly increased ionic conductivity of **LiOTf** compared to **Mix** demonstrates that the formation of metal-ligand coordination facilitates cation-anion dissociation and therefore improves the ionic conductivity of the PDMS (Figure 1d).

To provide critical molecular level insights that are hard to capture by experimental characterization techniques, fully atomistic molecular dynamics (MD) simulations are performed with the Large Atomic Molecular Massive Parallel Simulator (LAMMPS) (Figure 2a).[49]

The molecular interaction is described using the polymer-consistent force field (PCFF).[50] Each simulated system consists of 20 PDMS chains, each 21 monomers long, and 20 LiOTf molecules, equivalent to the experimentally characterized structure. A full description of the MD simulation methods is provided in the experimental section and supporting information (section 3). Results for the MD simulated **LiOTf** and **Mix** are given in Figure 2b-d and Figure 2e-g, respectively.

With the equilibrated MD system, we first compare the polymer-salt interaction in **LiOTf** and **Mix**. From the coordination matrices shown in Figure 2b and Figure 2e, Li^+ tends to interact with different electronegative moieties in the two system. In **LiOTf**, Li^+ has a strong tendency to coordinate both with the nitrogen atom on the pyridyl imine group and the oxygen atoms on OTf^-. In **Mix**, Li^+ preferably interacts with the oxygen atoms on OTf^-. It is worth noting that the most favorable lithium coordination is 4 and 5, consistent with previous work by Olsher et al.[51] The geometries of most 4-fold coordination and 5-fold coordination structures are found to be close to tetrahedral and square-pyramidal by visualization with Visual Molecular Dynamics (VMD) software.[52] In addition, the coordination matrix in Figure S11 indicates that Li^+ barely interacts with the siloxane group on the PDMS backbone. The coordination analysis based on simulation is consistent with our mass spectroscopy experimental result, confirming that the most probable structure is 4-fold coordination, which helps to validate the transferability of the PCFF force field to the PDMS and salt system.

To better understand the effect of metal-ligand coordination on ion and chain mobility, we investigate the diffusion coefficient of different components in the MD simulations of these two material systems. The MSD plots of ions and polymer chains for **LiOTf** are shown in Figure 2c. Both Li^+ and OTf^- motion is subdiffusive before 5 ns, i.e., $MSD \propto \tau^{\alpha}$ with $\alpha < 1$. At times longer than 5 ns, the ion motion becomes diffusive and the diffusion coefficient can be obtained from the MSD by applying the Einstein relation (Equation (1)). The OTf^- diffusion coefficient ($D_{OTf^-} = 1.12\ \mathring{A}^2/ns$) is larger than the Li^+ diffusion coefficient

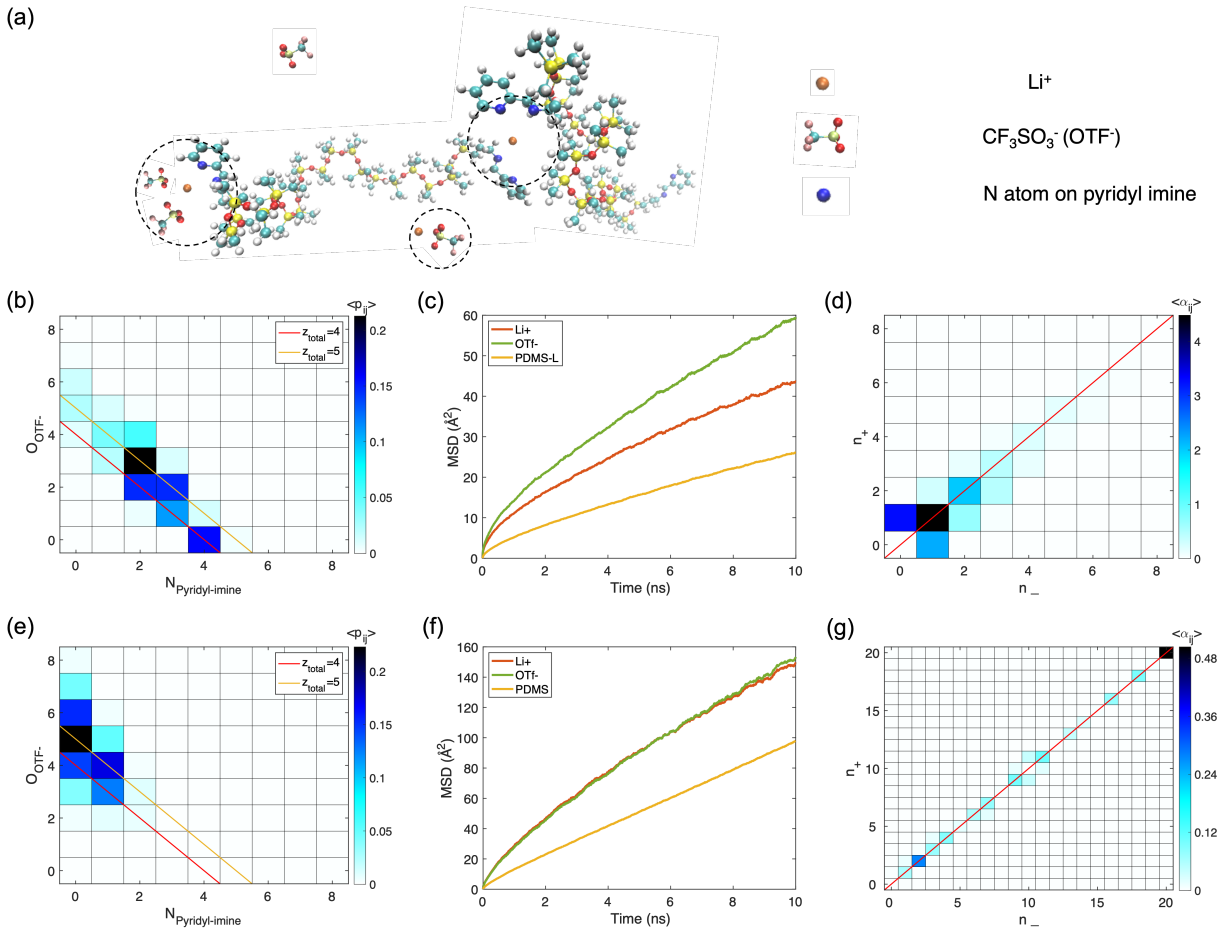

Figure 2: MD simulation. (a) Schematic representation of different Li^+ coordination environments for **LiOTf**. (b-d) show the results of **LiOTf** and (e-g) show the results of **Mix**: (b, e) coordination matrix that presents the relative contribution to the total coordination of Li^+ by oxygens from OTf^- and nitrogens from the end group of polymer chains. The grids passed through by the red and yellow line represents the most favorable total coordination number of 4 and 5. p_{ij} is the probability of each coordination combination over the simulation time. (c, f) MSD plot of cations, anions and polymer chains. (d, g) ion clustering statistics, where the grids passed through by the red line represents the neutral clusters. α_{ij} is the average counts of each cluster over the simulation period.

($D_{Li^+} = 0.84\ \mathring{A}^2/ns$). The results show that both cations and anions are mobile in the polymer matrix, with anions having higher mobility than cations. We infer that the motion of cations is mainly through the ligand exchange process, and is slowed down by this transient coordinating interaction; in contrast, anions are less confined and the motion is facilitated by chain segmental motion. The PDMS chains also diffuse over time, but at a much slower rate than the ions. For **Mix**, the MSD curves of cations and anions (Figure 2f) almost coincide,

with similar diffusion coefficients of $D_{Li^+} = 2.75\ \mathring{A}^2/ns$ and $D_{OTf^-} = 2.78\ \mathring{A}^2/ns$). This is due to the poor solvation ability of pristine PDMS, which promotes the formation of ionic clusters and results in the cations and anions diffusing together. Interestingly, the diffusion coefficients of both the ions and the chains in **Mix** are about three times larger than their values in **LiOTf**, resulting from the fact that ion motion in **Mix** encounters less confinement from the PDMS chains due to minimal coordination. At first glance, this seems contrary to our experimental results since ionic conductivity is typically thought to be directly related to the diffusion coefficient. However, the presence of ionic clusters instead of single ions significantly decreases the amount of charge carriers in the system, and therefore yields low ionic conductivity of the material.

Ion clustering is a common phenomenon at high salt concentration or when the interaction with the local structure is not strong enough for salt ionization, leading to correlated motion of cations and anions.[53] According to the cluster Nernst-Einstein (cNE) approach developed by Grossman et al, the net charge and diffusivity of each ionic cluster are aggregated to give the overall system conductivity (i.e. neutral clusters do not contribute to conductivity, Equation (3)).[34] The cluster populations of **LiOTf** and **Mix** are shown in Figure 2d and 2g, respectively. For **LiOTf**, both charged clusters and neutral clusters are observed at thermodynamic equilibrium, with clusters up to 12 ions (6 cations and 6 anions). For **Mix**, the cluster analysis shows an increase of cluster size, up to all ions in the simulation box (into a single cluster). The formation of very bulky neutral ionic clusters explains the lower ionic conductivity compared to that of **LiOTf** measured from experiments. More importantly, it demonstrates that by introducing ligands onto the polymer chains, the formation of metal-ligand coordination reduces large neutral ionic aggregates and facilitates the transport of charge carriers, improving the conductivity. Using the cNE equation (Equation (3)), we find conductivity for **LiOTf** is 0.0041 S/m while that for **Mix** is 0.00036 S/m. The ratio of the ionic conductivity with ligands to without is about 11.4 times, which matches well with the 17-times ratio from the experiments. Without the cluster correction on the NE equation,

the ionic conductivity would be 0.036 S/m and 0.11 S/m for **LiOTf** and **Mix**, which would contradict the experimental results. We note here that while our trends match well with experiments, our predicted conductivity values are substantially above the experimentally measured values. We believe this has to do with the scaled representation of the cation-anion interaction strength, which will be discussed in more depth when we compare results for different anions.

Next, we are interested in assessing whether interchain cation hopping via continuous ligand exchange is an important transport mechanism for cations. We suspect cation hopping might be important, because the MSD plots show that chain motion is 2-3 times slower than Li^+ diffusion, indicating that cation diffusion, on this timescale, is not solely driven by the segmental motion of the polymer. The hopping behavior varies considerably among individual cations. In Figure S7 and Figure S8 we show the behavior of two example ions: the less diffusive Li^+ tends to attach to one ligand from one chain over 80 ns while exchanging among other ligands from different chains; the more diffusive Li^+ hops frequently between chains. It is also shown in Figure S9 that Li^+ jumping among polymer chains is more frequent in **Mix** than in **LiOTf**, due to the weak polymer-ion interaction and hence short residence time when there is no ligand. In addition, the motion of Li^+ along the host chain is insignificant for this material system, contrary to other polymer-salt systems like PEO electrolytes,[54] because only the ligand grafted on the ends of the chains can coordinate with the lithium ions while the monomers hardly interact with Li^+ due to the non-polar nature of PDMS. The radial distribution function (RDF) plot of oxygens within the PDMS backbone relative to the lithium ions supports this lack of association with an average coordination number of zero (Figure S12).

The effect of counter anions

Since varying the counter anion in a metal-ligand complex can yield distinct coordination strength and lifetime, a series of Li^+ coordinated PDMS with different anion species is synthe-

sized to study the influence of counter ions on ionic conductivity.[20,55] Another three Li salts, lithium chloride (LiCl), lithium tetrafluoroborate ($LiBF_4$), and lithium bis(trifluoromethanesulfonyl)imide (LiTFSi) are added into the ligand functionalized PDMS at the same 1:1 molar ratio (**LiCl**, **$LiBF_4$**, and **LiTFSi**, respectively), which show distinct solubilities after rigorous mixing. **LiCl** has a large amount of undissolved salt at the bottom of the container. **$LiBF_4$** also has an observable amount of undissolved salt left after thorough mixing. **LiTFSi** is fully dissolved in the PDMS oil and yields a more viscous liquid with darker color than **LiOTf** (Figure 3a). The differences among the Li^+ coordinated PDMS containing different counter anions can also be seen from their IR spectra (Figure 3b). Comparing to the spectrum of **PDMS-L**, the C=N stretching peak at the wavenumber of 1650 cm^{-1} is partially shifted to 1593 cm^{-1} due to the formation of Li^+-pyridyl imine coordination in the spectrum of **LiTFSi**.[56] The peaks at the wavenumber of $1300 - 1380 cm^{-1}$ are from the overlapped C-F and S=O bond stretching in $TFSi^-$ anions.[57] Conversely, the spectra of **LiCl** and **LiBF4** are quite similar to **PDMS-L**; the peak shift caused by coordination and the presence of counter anions are barely detectable.

The ionic conductivity of the Li^+ coordinated PDMS with different counter anions is measured by EIS and shows orders of magnitude differences: **LiCl** < **$LiBF_4$** < **LiOTf** < **LiTFSi** (Figure 3c, Figure S13, Table S3). The ionic conductivity of the Li^+ coordinated PDMS increases with the size of the counter anion. Bulkier counter anions such as OTf^- and $TFSi^-$ have higher charge delocalization, yielding weaker cation-anion interaction, and therefore the increased ion mobility promotes higher ionic conductivity.[39] In contrast, the smaller anions such as Cl^- and BF_4^- have stronger electrostatic attraction with Li^+, which results in more significant cation-anion association.[58] This explains the limited salt solubility in PDMS, and moreover, the low ion concentration and low ion mobility together lead to the low ionic conductivity. The MD simulations of **LiTFSi** also show greater ionic conductivity than **LiOTf** ($\sigma_{TFSi^-} = 0.0054\ S/m$ vs $\sigma_{OTf^-} = 0.0041\ S/m$), though the trend is less prominent than the experimental one. At 30 ℃, the ionic conductivity from MD simulations

for **LiTFSi** is about 3 times higher than the experimental value and it is about 46 times higher than the experimental value for **LiOTf**. The reason for the large discrepancy in **LiOTf** could be the underestimation of ionic correlation strength due to the use of scaling charge factor, leading to greater diffusivity as molecular sizes decrease.

To gain a more quantitative insight into the mobility of the PDMS chain and counter anions, Pulsed-field-gradient (PFG) spin-echo (SE) NMR is performed to investigate the self-diffusion of the system.[23,59] The dynamics of PDMS chain is quantified based on the stimulated-echo signal attenuation of ^{1}H spectra (note: the self-diffusion coefficient of ^{1}H is not quantitatively identical to the self-diffusion coefficient of PDMS chain but they are strongly correlated), and the self-diffusion coefficient of counter anions is calculated from the stimulated-echo signal attenuation of ^{19}F (Figure 3d, Figure S14, Figure S15, and Table S4).[23,60] It is worth noting that since the PDMS samples are not diluted by any solvent, the self-diffusion coefficients measured directly reflect the actual dynamics of the material. Comparing the diffusion coefficients in **LiOTf** and **LiTFSi**, we can see that the mobility of the hydrogens on the PDMS chains is similar in **LiTFSi** and **LiOTf**, whereas the mobilities of counter anions are quite different: $TFSi^-$ is higher than OTf^-. MD simulations of **LiTFSi** compared to **LiOTf** show that the bulkier, less polar $TFSi^-$ anion tends to have more frequent intercluster hopping, leading to an overall higher diffusivity ($D_{TFSi^-} = 1.66\ \mathring{A}^2/ns, D_{Li^+} = 1.26\ \mathring{A}^2/ns$). The cluster analysis from MD observations is provided in Figure S17, which is consistent with previous work on PEO-LiTFSi systems: there are mostly neutral ion pairs, but also a non-negligible concentration of negatively charged clusters, resulting in an overall asymmetric distribution.[61] The distribution of charged clusters in **LiTFSi** is less symmetric compared to that of **LiOTf**, with overall more negatively charged clusters present in the system, indicating that Li^+ from **LiTFSi** interacts more strongly with the polymer chains. Furthermore, the diffusion coefficients of positively charged clusters tend to be slightly smaller than those of negatively charged clusters with the same constituent number of ions, due to the stronger local interaction between positively

charged clusters and electronegative ligands on the polymer.

The ionic conductivity of **LiOTf** and **LiTFSi** as a function of the ambient temperature T from 0 ℃ to 100 ℃ (Figure 3e and Figure S16) is measured experimentally. The logarithmic scale of ionic conductivity is found to be linearly proportional to $1000/T$, following an Arrhenius behavior $\sigma \sim exp(-E_a/RT)$, where E_a is an apparent activation energy, R is the universal gas constant, and T is the absolute temperature.[59,62] The apparent activation energy is the slope of the fit line, which is quite similar in **LiOTf** and **LiTFSi**. We believe that the apparent activation energy is the combination of the energy barriers of (1) the cation-anion interaction of the Li salt and ion clusters; (2) dissociation of Li^+ from the connected ligands; and (3) the self-diffusion of PDMS chain that facilitates ion motion.[11,36,59]

The effect of ion concentration

We study the effect of ion concentration on the ionic conductivity of the model system by preparing a series of LiOTf and LiTFSi coordinated PDMS with different salt concentrations (**LiOTf0.2** to **LiOTf1.4** and **LiTFSi0.2** to **LiTFSi1.4**, the number in the sample name indicates the mole ratio of PDMS:LiOTf= $1 : n$ for formulations that deviate from 1 : 1). In both cases, the ionic conductivity of the PDMS complex first increases and then decreases as the Li salt concentration increases; the highest ionic conductivity is reached at around the maximum coordination capacity of the ligands with Li^+ cations (corresponding to PDMS:Li salt= 1 : 1 in Figure 3f, Table S6). This indicates that at first, more Li^+ cations and counter anions exist in the system as the Li salt concentration is increased, improving the ionic conductivity. However, when the ligand coordination capacity is oversaturated by excess Li salt, the ionic conductivity of the PDMS complex starts to decrease monotonically (Figure S18). As both seen from the previous studies and our MD simulation (Figure S19), ion pairs and higher-order clusters form at high Li salt concentration, which hinders the effective cation-anion dissociation and ion transport, thereby decreasing the overall ionic conductivity.[32,62,63]

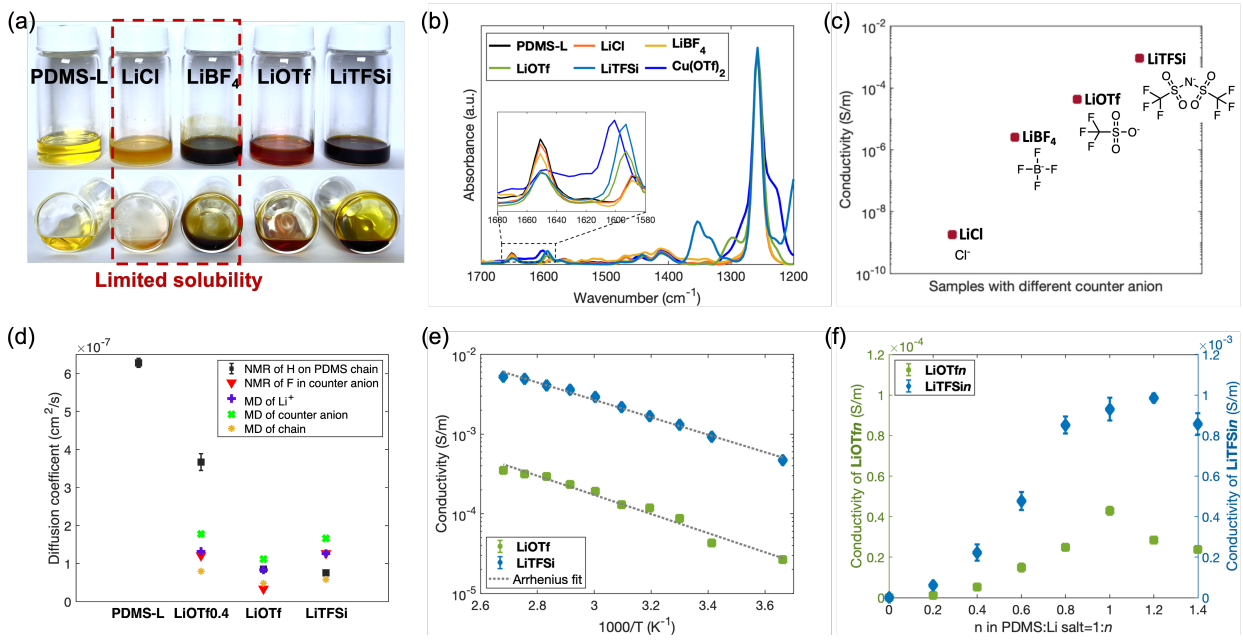

Figure 3: Li^+ coordinated PDMS. (a) Both front view and bottom view photos of the ligand-functionalized PDMS and the Li^+ coordinated PDMS containing different counter anions. **LiCl** and **$LiBF_4$** have undissolved salt at the bottom of the vials, whereas **LiOTf** and **LiTFSi** yield a clear product. (b) IR spectra of the PDMS precursor and the metal coordinated PDMS. (c) Ionic conductivity of the Li^+ coordinated PDMS with varying counter anions. (d) A comparison of diffusion coefficients from both experimental and simulation results: diffusion coefficients of ^{1}H from PDMS chain and ^{19}F from counter anion in Li salts are obtained from PFG SE NMR measurements at 100 ℃, and diffusion coefficients of Li^+ and counter anions are obtained from MD simulation at 30 ℃. Error bars are calculated from ^{1}H in different moieties on the PDMS chain. (e) Ionic conductivity as a function of temperature for **LiOTf** and **LiTFSi**. (f) Ionic conductivity of LiOTf and LiTFSi coordinated PDMS with varying salt concentration.

We can look more deeply into the mechanism for the salt concentration dependence with PFG SE NMR and MD simulations. It can been clearly seen from the trend of **PDMS-L**, **LiOTf0.4**, and **LiOTf**, that the segmental motion of PDMS chain slows down when forming complexes with LiOTf, and decreases further at higher LiOTf concentration (Figure 3d), because the formation of metal-ligand coordination adds temporary constraints to the chain ends.[19] The diffusion of OTf^- also slows down at higher LiOTf concentration, confirming that the anion motion is associated with the chain motion. The MD calculated diffusion of the anions follows the same trends as the NMR results. The MSD plots from MD simulations (Figure S19) also show that the mobility of both the ions and the chain decrease with higher

salt concentration. Therefore, when the PDMS is oversaturated by Li salt, both clustering and reduced segmental motion can inhibit the overall ionic conductivity of the material. In this particular material system, chain mobility seems to be a secondary effect since the peak conductivity occurs near a molar ratio of 1:1, which clearly has reduced chain mobility.

The effect of cation identity

We next study the effect of coordination strength on the ionic conductivity of the metal-ligand coordinated PDMS by using a multivalent cation, Cu^{2+}. To obtain the coordination structure, a small-molecule Cu^{2+}-pyrdiyl imine complex is synthesized by adding copper trifluoromethanesulfonate ($Cu(OTf)_2$) into the model ligand N-propyl(2-pyridyl)methanimine. The molecular weight of the complex is analyzed by MS in ESI positive ion mode and found to be 689.05 Da, confirming the ratio between Cu^{2+} and pyridyl imine ligand is 1 : 2 (Figure S4).[20,64] A series of $Cu(OTf)_2$ coordinated PDMS with different salt concentrations is synthesized (**Cu(OTf)$_2$0.2** to **Cu(OTf)$_2$**, the number in the sample name indicates the mole ratio of PDMS:$Cu(OTf)_2 = 1 : n$ for formulations that deviate from 1 : 1). We expect that Cu^{2+} forms a stronger and more stable complex than Li^+, yielding a less dynamic network, which can be characterized by the rheology of the PDMS complexes. The linear viscoelastic (LVE) region of each material is first determined by running a strain sweep at a frequency of 1 Hz (Figure S20),[65] which shows that the critical strain of **Cu(OTf)$_2$** is near 1%. An oscillation strain of 0.1% is therefore chosen to perform the frequency sweep for all the samples (Figure 4a). We first compare the coordination strength of Li^+ and Cu^{2+} by examining the rheological curves of **LiOTf** and **Cu(OTf)$_2$**: the storage and loss moduli (G' and G'', respectively) of **Cu(OTf)$_2$** are orders of magnitude higher than the moduli of **LiOTf$_2$** within the full frequency range measured. In **Cu(OTf)$_2$**, $G' > G''$ and G' remains independent of the frequency, indicating that the material is in the rubbery plateau region due to the presence of strong metal-ligand coordination, which act as transient crosslinks in the polymer; whereas in **LiOTf**, $G' < G''$, indicating that the material is in the terminal region, where

chains relax quickly and the material behaves like a viscoelastic fluid.[66] The difference in viscoelasticity of the Li^+ and Cu^{2+} coordinated PDMS can also be directly seen from the photos of **LiOTf** and **Cu(OTf)$_2$** samples: the former is a viscous liquid and the later is a flexible film, confirming that Cu^{2+} yields much stronger bonding with the ligand functionalized PDMS than Li^+. The variation of polymer viscoelasticity of the Cu^{2+}-coordinated PDMS as a function of $Cu(OTf)_2$ concentration is also shown in the rheology plot: the material transforms from a viscoelastic fluid to a viscoelastic solid with increasing $Cu(OTf)_2$ concentration. A crossover between the storage and loss modulus arises and shifts to the lower frequency at the higher $Cu(OTf)_2$ concentration, indicating that the characteristic relaxation time of the PDMS is significantly prolonged when it is crosslinked by $Cu(OTf)_2$.[19] The change in polymer dynamics caused by using the more strongly coordinated Cu^{2+} or increasing the Cu salt concentration also results in the increase of T_g, which is measured by differential scanning calorimetry (DSC) (Figure 4b). The T_g of **LiOTf**, **Cu(OTf)$_2$0.2**, and **Cu(OTf)$_2$0.4** is below the testing limit of the machine (-90 ℃), so no slope change is seen on the heat flow curve. However, the T_g of **Cu(OTf)$_2$0.6**, **Cu(OTf)$_2$0.8**, and **Cu(OTf)$_2$** increases to around -38 ℃, -30 ℃, and -28 ℃, respectively. The dramatic increase in T_g reflects the reduction of chain mobility, which should confine the ion transport.[59,67]

To study how the coupled Cu^{2+} ion concentration and network dynamics together effect the ionic conductivity of the material, we measure the ionic conductivity of the PDMS complex as a function of $Cu(OTf)_2$ concentration, showing quite a different trend than in the Li^+ coordinated system (Figure 4c). We note that the $Cu(OTf)_2$ coordinated PDMS, regardless of salt concentration, cannot achieve nearly as high conductivity as the maximum value of the LiOTf coordinated PDMS. The maximum ionic conductivity is obtained at **Cu(OTf)$_2$0.4**, which is far lower than the maximum coordination capacity. In addition, a drastic decrease of the ionic conductivity is observed beyond this peak. This trend can be well correlated to the change in the rheological behavior and the glass transition temperature with increasing $Cu(OTf)_2$ concentration. At low $Cu(OTf)_2$ concentrations, the PDMS complex

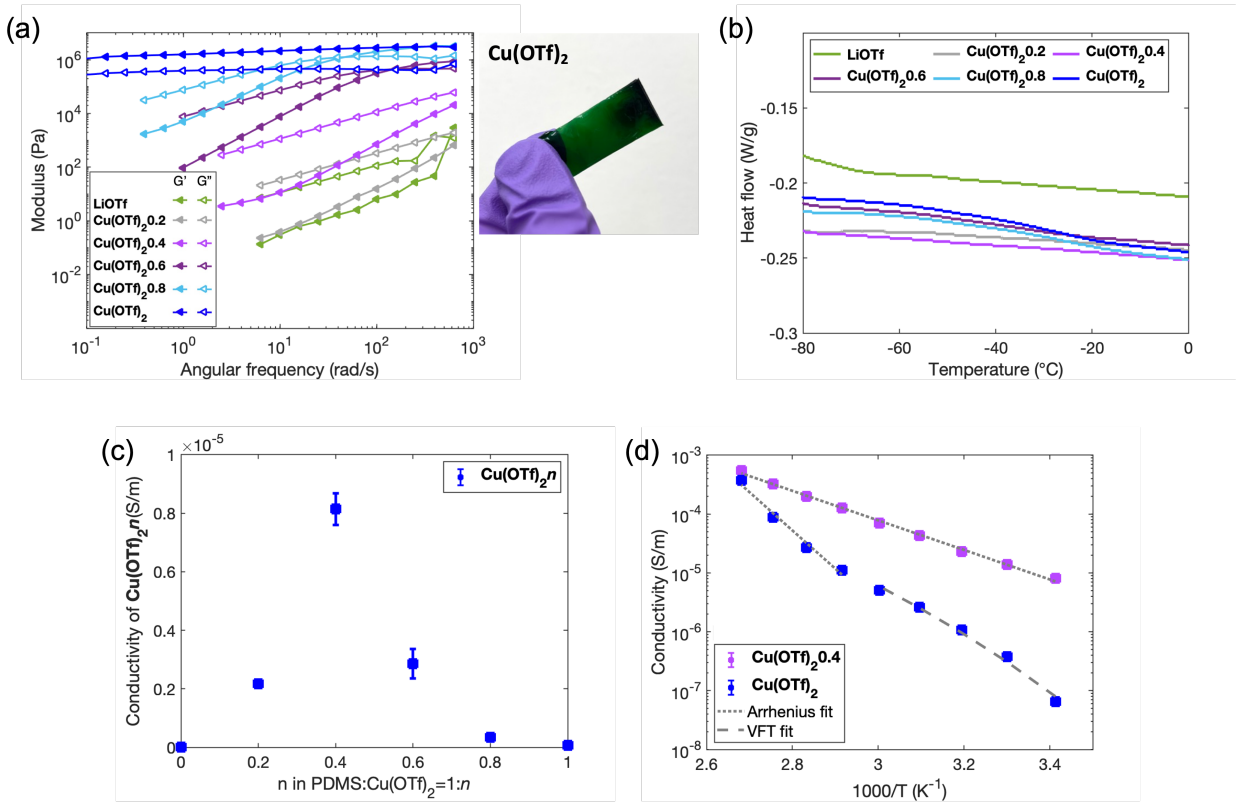

Figure 4: Cu^{2+} coordinated PDMS with different salt concentration. (a) Frequency sweeps at the strain of 0.1% measured by rheology, and a photo of a piece of $\mathbf{Cu(OTf)_2}$. (b) DSC curves of different PDMS complexes. (c) The variation of ionic conductivity of the polymer. (d) Ionic conductivity as a function of temperature for $\mathbf{Cu(OTf)_2}z$.

is still fluid and its glass transition temperature is far below the room temperature ($T > T_g$+100 °C), so the fast chain segmental motion facilities the ion motion at room temperature, which is similar to the Li^+ coordinated system. Increasing $Cu(OTf)_2$ concentration from $\mathbf{Cu(OTf)_20.2}$ to $\mathbf{Cu(OTf)_20.4}$ improves the ion concentration and therefore increases the ionic conductivity of the material. However, the trend is interrupted by the slowing of polymer dynamics in the system at higher $Cu(OTf)_2$ concentration. For $\mathbf{Cu(OTf)_20.6}$, $\mathbf{Cu(OTf)_20.8}$, and $\mathbf{Cu(OTf)_2}$, the ion motion slows down due to the significantly extended chain relaxation. Another interesting observation is that the Cu^{2+} system is more ionically conductive than the Li^+ system at the low salt concentration of PDMS:salt=1 : 0.2 and 1 : 0.4 (Figure S22). This can be attributed to the valency of the metal cation: Cu^{2+} is balanced by two OTf^- anions whereas Li^+ only has one, so when adding the same number

of moles of LiOTf and $Cu(OTf)_2$ salt into the PDMS, the ion concentration is higher in the Cu^{2+} system than the Li^+ system, which promotes the high ionic conductivity.

We then compare the ionic conductivity change as a function of temperature in both **$Cu(OTf)_2$0.4** and **$Cu(OTf)_2$** (Figure 4d, Figure S23). **$Cu(OTf)_2$0.4** shows an Arrhenius relation similar to the Li^+ system as discussed in the previous session, but with a much higher apparent activation energy, which likely results from a combination of the stronger metal-ligand interaction and slower network dynamics suppressing the ion transport in the Cu^{2+} coordinated PDMS compared to the Li^+ counterpart. However, **$Cu(OTf)_2$** behaves differently, there is an apparent trend change at around $T = T_g + 100$ ℃. Given that the Arrhenius relation between ionic conductivity and temperature is valid for a temperature range of $T > T_g + 100$ ℃, whereas the Vogel–Fulcher–Tammann (VFT) relation is valid for temperature range of $T_g < T < T_g + 100$ ℃, we believe that the factors governing the ion transport in **$Cu(OTf)_2$** vary at different temperature ranges. At high temperatures, PDMS chain motion is prompt, and thus Arrhenius activation energy is dominated by the strength of ion correlation and metal-ligand coordination. At low temperatures, ion diffusion is strongly coupled with chain mobility.[59,68–71]

The synergistic effect of coordinating PDMS with Cu^{2+} and Li^{1+}

So far, the study of the Li^+ coordinated PDMS and the Cu^{2+} coordinated PDMS shows that the maximum ionic conductivity of each system appears at a different coordination ratio: the Li^+ system shows the highest ionic conductivity near the saturation point, whereas the Cu^{2+} system shows the highest ionic conductivity at a much lower coordination ratio. Moreover, Cu^{2+} generates higher ionic conductivity than Li^+ when both of them are at the same low salt concentration (the ratio of PDMS:salt=1 : 0.2 and 1 : 0.4), because of the doubled concentration of counter anions added into the system. Given these results, a mixed Li^+ and Cu^{2+} coordinated system with large portion of Li^+ and small portion of Cu^{2+} could not only increase the ionic conductivity of the material but also enhance the mechanical properties.

To verify this idea, we generate a series of ligand functionalized PDMS with both Li^+ and Cu^{2+}, and study the rheological behavior as well as the ionic conductivity of the material by varying the ratio between LiOTf and $Cu(OTf)_2$ (**Li0.8Cu0.2** to **Li0.2Cu0.8**, the numbers after each metal indicates the mole ratio of PDMS:LiOTf:$Cu(OTf)_2 = 1 : m : n$). From the rheology plots, we see that the viscoelasticity of the mixed ion coordinated PDMS is similar to the Cu^{2+} coordinated PDMS at the same salt concentration, because the much stronger coordination of Cu^{2+} compared to Li^+ dominates the relaxation of the dynamic network (Figure 5a). A synergistic effect appears as expected when using $Cu(OTf)_2$ to replace a small amount of LiOTf in the coordinated PDMS; **Li0.8Cu0.2** shows higher ionic conductivity as well storage and loss moduli than **LiOTf** (Figure 5b).

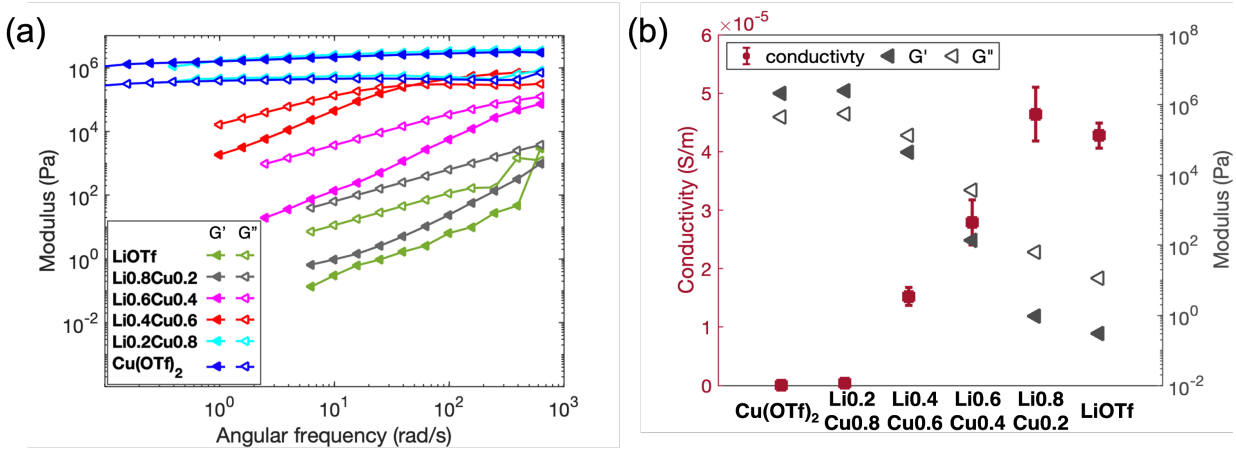

Figure 5: PDMS coordinated by mixed Li^+ and Cu^{2+} ions. (a) Frequency sweeps at the strain of 0.1% measured by rheology. (b) Ionic conductivity of the PDMS in different ratios of Li^+ and Cu^{2+}, and the storage and loss moduli extracted from the frequency sweeps at 10 rad/s.

Conclusions

In this work, we investigate the ion conductivity mechanism of a metal-ligand coordinated polymer by designing of the model system consisting of pyridyl imine functionalized PDMS and two metal cations Li^+ and Cu^{2+}. We first confirm that the formation of metal-ligand complex promotes ion dissociation in the polymer matrix by showing increased ionic conduc-

tivity of the ligand-functionalized PDMS compared to the pristine PDMS. MD simulations prove that cation-anion dissociation is facilitated by the interaction of metal cations and ligands attached to the polymer. Based on this finding, a series of Li^+ coordinated PDMS with different counter anions of the salt are synthesized to investigate the effect of cation-anion interactions on the ionic conductivity of the polymer. We find that a bulkier anion not only yields the stronger Li^+-ligand coordination but also suppresses the tendency for ion precipitation, promoting higher ionic conductivity. In addition, MD simulations show that bulkier anions with higher delocalized charge tend to have more frequent intercluster hopping and form more negatively charged clusters. The effect of salt concentration is next studied, which is seen to first enhance the ionic conductivity of the complex by increasing the ion concentration. However, for the Li^+ cation systems, the ionic conductivity reaches the maximum when the ligand coordination capacity is saturated, and then starts to decrease at the higher salt concentrations since the additional salt preferentially forms clusters. MD simulations confirm that the chain segmental motion is also hindered by increasing salt loading, though this seemed to be of secondary influence for the Li^+ system. The temperature-dependent ionic conductivity of the Li^+ coordinated PDMS shows an Arrhenius relation, indicating that the strength of metal-ligand coordination and cation-anion interaction are the rate-determining factors in the ion transport.

To investigate the effect of coordination strength on the ionic conductivity of the polymer, a series of Cu^{2+} coordinated PDMS with different salt concentration is synthesized. From the rheological measurements, we show that as expected, Cu^{2+} forms a much stronger coordination with the ligand on the PDMS than Li^+. The Cu^{2+} coordinated PDMS transforms from a viscoelastic fluid to an elastic solid as the salt concentration increases, accompanied by a significant rise of T_g, indicating a rapid decrease of polymer dynamics. The ionic conductivity of the complex first increases with the $Cu(OTf)_2$ concentration, but soon reaches the maximum at a low coordination ratio. Further increasing $Cu(OTf)_2$ concentration leads to a sharp decrease in ionic conductivity. We attribute this to the reduction of chain mobility in

the system, which limits the ion transport. In addition, at the same low salt concentration, Cu^{2+} coordinated PDMS exhibits higher ionic conductivity than Li^{+} coordinated PDMS due to the doubled concentration of mobile anions. This importance of reduced chain mobility is in contrast to its minor role in the Li^{+} coordinated material. Based on these findings, an optimized metal-ligand coordinated PDMS with higher ionic conductivity and improved mechanical strength is achieved by a combination of high Li^{+} and low Cu^{2+} concentration in the system. This paper explores the structure-property relationship of the metal-ligand coordinated PDMS as a novel polymer electrolyte. At a superficial level the governing mechanisms are similar to other polymer electrolytes – salt solvation, chain mobility, ion clustering, ion diffusion, and ion hopping – however, their relative importance and how they are controlled by the polymer structure and salt selection are quite distinct. These insights will enable more strategic future material design of low T_g ionically conductive polymers.

Experimental section

Synthesis of model ligand N-propyl(2-pyridyl)methanimine. The model ligand N-propyl(2-pyridyl)methanimine is synthesized via a one-step condensation reaction. Under vigorous stirring at room temperature, propylamine (5.9 g, 0.1 mol) is added dropwise into a 50 ml round-bottom flask containing 2-pyridinecarboxaldehyde (10.7 g, 0.1 mol). 3A molecular sieves are added into the mixture to adsorb water. The system is reacted overnight, and the product is filtered to remove the molecular sieves, obtaining yellow colored liquid (11.2 g, yield 73%). ^{1}H NMR: (50 MHz, $CDCl_3$) δ 8.62 (ddd, J = 4.9, 1.4, 1.4 Hz, 1H), 8.36 (t, J = 1.6 Hz, 1H), 7.97 (s, 1H), 7.72 (ddd, J = 7.6, 7.6, 1.7 Hz, 1H), 7.29 (ddd, J = 7.5, 4.8, 1.2 Hz, 1H), 3.63 (t, J = 6.9 Hz, 2H), 1.74 (qt, J = 7.2 Hz, 2H), 0.95 (t, J = 7.4 Hz, 3H) (Figure S2).

Synthesis of coordination complex LiOTf-N-propyl(2-pyridyl)methanimine. LiOTf salt (0.39 g, 0.0025 mol) is dissolved in methanol (5 ml), and N-propyl(2-pyridyl)methanimine

(0.74 g, 0.005 mol) is added into the solution. The mixture is stirred for 1 hr followed by evaporating the methanol.

Synthesis of pyridyl imine functionalized PDMS (PDMS-L). PDMS-L is synthesized following a previously published procedure with slight modification.[42] Aminopropyl terminated polydimethylsiloxane (50g, 0.03mol, the molecular weight is estimated from ^{1}H NMR spectrum) and 2-pyridinecarboxaldehyde (7.5 g, 0.07 mol) are added into a 200 ml round-bottom flask equipped with a magnetic stir bar. Dichloromethane (50ml) is added into the mixture as a solvent, and molecular sieves 3A (10 g) are used to adsorb water generated. The reaction proceeded at room temperature for 24 hr. The mixture is then filtered to remove the molecular sieves. The obtained solution is dried under rotary evaporation to remove dichloromethane. The product is then redissolved in hexane (20 ml) and extracted by acetonitrile (50 ml) to remove excess 2-pyridinecarboxaldehyde, and the extraction is performed three times. The solution is dried under rotary evaporation to remove hexane, and then left in a vacuum oven at 100 ℃ for 12 hr to completely remove the residual solvent. The product is filtered through a 0.45 μm PTFE filter, obtaining yellow colored PDMS oil (46 g, yield 81%). ^{1}H NMR: (50 MHz, $CDCl_3$) δ 8.67 (dt, J = 4.9, 1.4 Hz, 1H), 8.39 (t, J = 1.5 Hz, 1H), 8.01 (dt, J = 7.9, 1.1 Hz, 1H), 7.76 (td, J = 7.7, 1.8 Hz, 1H), 3.69 (td, J = 7.1, 1.4 Hz, 2H), 1.78 (ddd, J = 7.2, 6.0, 3.6 Hz, 2H), 0.68-0.52 (m, 2H), 0.09 (d, J = 2.4 Hz, 69H) (Figure S1). The molecular weight of **PDMS-L** is calculated based on the integration of peaks: $69 \div 3 \times 74 + 147 \times 2 \approx 2000\ g/mol$.

Synthesis of metal coordinated PDMS. A vial equipped with a stir bar is used for sample preparation. In the preparation of Li^+ coordinated PDMS, the calculated amount of Li salt is weighed and added into the pyridyl imine functionalized PDMS oil and the mixture is stirred overnight. LiCl and $LiBF_4$ are not fully dissolved in the PDMS at a molar ratio of PDMS:Li salt= 1 : 1 even after being stirred at elevated temperature for a day. We also prepare LiCl and $LiBF_4$ coordinated PDMS samples with additional solvents to facilitate the dissolution. Although a transparent solution is obtained with the presence of solvents,

the salt precipitates out after solvent evaporation. In the preparation of Cu^{2+} coordinated PDMS, THF is used to dissolve the calculated amount of $Cu(OTf)_2$ salt and the solution is added into the PDMS oil dropwise under vigorous stirring. The mixture is stirred for 2 hr to ensure a thorough mixing. The solution is cast into a Teflon mold, followed by evaporating the solvent. Then the sample is transferred into a vacuum oven and dried for 24 hr to ensure the complete removal of the solvent.

^{1}H nuclear magnetic resonance (^{1}H NMR). The ^{1}H NMR spectrum of the ligand functionalized PDMS is acquired on a Bruker AVIII HD 500 MHz spectrometer equipped with a liquid-nitrogen cooled cryoprobe. The polymer is dissolved in $CDCl_3$ and processed by 16 scans, with 90° excitation and 30 s relaxation delay. Data are plotted in MNova (Mestrelab Research).

Liquid chromatography–mass spectrometry (LC-MS). The coordination complex LiOTf-N-propyl(2-pyridyl)methanimine is dissolved in methanol (5 $wt/wt\%$) and then using tee-in direct injection into the mass spectrometer with a flow rate of 200 $\nu l/min$. The flow rate of the sample through the syringe pump is 9 $\nu l/min$. Sciex X500B is operated in electrospray ionisation (ESI) positive ion fourier transform (FT) mode, and the calibration is done with positive calibrant. ESI voltage is 5.5 kV, source temperature is 300 ℃, declustering potential is 50 V, accumulation time is 0.15 s. An MS full scan from m/z 100 to m/z 1000 in profile mode acquired from 0 min to 5 min. Time-of-flight mass spectrometry (TOF MS/MS) is also acquired at the mass range of m/z 100 to m/z 1000 from 0 min to 5 min.

Fourier-transform infrared (FTIR) spectroscopy. The IR spectra of the materials are collected by a Bruker Vertex V80V Vacuum FTIR system under the attenuated total reflection (ATR) configuration. The spectral range of 4000 cm^{-1} to 600 cm^{-1} are collected.

Electrochemical Impedance Spectroscopy (EIS). The metal-ligand coordinated PDMS samples are sandwiched between two pieces of gold coated SiO_2 substrates with 100 μm Teflon sheet spacers placed on both sides. The gold electrode had an area of $1cm^2$. The

samples are characterized with the Reference 3000AE potentiostat from Gamry Instruments. A sinusoidal voltage with an amplitude of 50 mV is applied in the frequency range of $1Hz$ to $1MHz$. Ionic conductivity of each polymer is calculated from the frequency with minimum phase angle shift read from Gamry's Echem Analyst software.

Pulsed-field-gradient (PFG) spin-echo (SE) NMR. Diffusion experiments are performed on a Varian INOVA 600 spectrometer operating at 599.50 and 564.01 MHz for ^{1}H and ^{19}F observation, respectively, equipped with a Nalorac broadband H/F probe with a double tuned outer coil. All experiments are performed at 100 ℃ to obtain good signals and all the samples of PDMS complex are directly injected into the NMR tubes without adding solvent. ^{1}H diffusion experiments are performed with the convection-compensated, bipolar-gradient double stimulated-echo (Dbppste_cc) pulse sequence, modified to include a 5 ms longitudinal eddy current delay. 16 gradient values are collected with 2 steady-state scans and 4 scans for each increment. Acquisition time is 1.3 s and relaxation delay is 4 s. Diffusion gradient pulse length (δ) is 4 ms and the diffusion delay (Δ) is 200 to 800 ms to ensure that at least three half-lives are acquired. ^{19}F diffusion experiments are performed with the convection-compensated double stimulated-echo (DgcsteSL_cc) pulse sequence. 16 gradient values are collected with 2 steady-state scans and 4 scans for each increment. Acquisition time is 1.0 s and relaxation delay is 2 s. Diffusion gradient pulse length (δ) is between 3 to 4 ms and the diffusion delay (Δ) is 750 to 1500 ms to ensure that at least three half-lives are acquired. Data is analyzed in MNova (Mestrelab Research). The diffusion coefficient of PDMS backbone in each sample is calculated based on a single exponential fit of the change of peak area integral in the ^{1}H diffusion experiment, and an average of the diffusion coefficients calculated from different peaks representing different moieties is used as the final value. The diffusion coefficient of counter anions in each sample is calculated based on a single exponential fit of the change of peak area integral in the ^{1}9F diffusion experiment.

Rheology. The rheology of the materials are measured by a TA Instruments DHR-3 rheome-

ter with a 40 mm-diameter parallel plate. $\sim 1.26\ ml$ sample is added to the stage with 2 mm thickness. Before each measurement, the sample is first equilibrated at 25 ℃ for sufficient period of time. In a strain sweep, 1 Hz frequency is performed. In a frequency sweep, 0.1% strain amplitude is performed.

Differential scanning calorimeter (DSC). The glass transition temperature of the polymer is tested by a TA Instruments DSC Auto 2500. The samples are loaded in Tzero aluminum pans and measured with a heating rate of 10 ℃/min and a cooling rate of 5 ℃/min from -90 ℃ to 120 ℃ for one heating-cooling-heating cycle. Data from the second heating process is used. Glass transition temperature of each sample (T_g) is determined from the midpoint of the transition on the heat flow curve.

Molecular dynamics simulation setup and equilibration. The fully atomistic MD simulations are performed with LAMMPS. Each simulated system consists of 20 PDMS chains, each with 21 monomers long, 20 salt pairs are doped into the system for PDMS:salt= $1:1$ case. For each salt species, we considered 9 randomized trajectories from 3 different initial configuration and 3 different initial velocity seeds.[72]

Force field parameters and initial configurations for the PDMS and ions are generated with the Enhanced Monte Carlo software[73] using the PCFF framework.[50] The point charge assigned to the ion pairs is rescaled by 0.7. The charge downscale procedure is commonly used for classical force field where a static point-charge model can lead to an exaggeration of ionic interaction strength.[74] The velocity-Verlet integrator with a time step of 0.5 fs is used for motion evolution; this value is selected as the largest one ensuring the reasonable drift of atoms within a single time step. The relaxation process consists of steepest descent and conjugate gradient energy minimization, followed by equilibration in the canonical (nVT) and isothermal-isobaric (nPT) statistical ensembles at the target temperature and pressure of 303 K and 1 bar, for a total duration of 5 ns. The Nose-Hoover thermostats and barostats are used with damping parameters set to 50 and 500 fs, respectively. The production run is conducted in the nVT ensemble at 303 K for 50 ns. For non-bonded interactions,

long-range electrostatic interactions are calculated by using the particle-particle particle-mesh solver with a 1.2 nm cutoff distance while Lennard-Jones interactions are truncated at 1.2 nm with the long-range Van der Waals tail corrections included for energy and pressure modification.

Molecular dynamics cluster and ionic conductivity analysis. The self-diffusion coefficient is calculated using the Einstein relation:

$$D_{ion} = \lim_{t\to\infty} \frac{\left\langle \frac{1}{N}\sum_{i=1}^{N} |\mathbf{x}_i(t_0+t) - \mathbf{x}_i(t_0)|^2 \right\rangle_{c,t_0}}{6t} \tag{1}$$

where $\mathbf{x}_i(t)$ is the instantaneous position of i^{th} particle at time t and N is the number of particles. The numerator is mean-squared displacement (MSD) of a molecule center of mass during time t and $\langle ... \rangle$ denotes an ensemble average. Note that we performed both configuration averaging and time-origin averaging using a sliding-window strategy. The relation only holds for the Fickian regime of the MSD curve, therefore, it is necessary to reach the diffusive linear regime to extract an accurate diffusion coefficient.[75]

With the diffusion coefficients for mobile species obtained from MSD, we first calculate the ionic conductivity with the Nernst-Einstein equation, which states that the total conductivity is proportional to individual diffusion coefficient and ionic concentration:

$$\sigma_{NE} = \frac{e^2}{Vk_BT}(N_+ z^2{}_+ D_+ + N_- z^2{}_- D_-) \tag{2}$$

where k_B is the Boltzmann constant, e is the elementary charge, V is the volume of simulation box, T is the temperature, $z_\pm$ and $N_\pm$ is the charge and number of cations and anions. However, the NE equation assumes ions do not interact with themselves, and is therefore only exact in the infinite dilution limit. For electrolytes with high salt concentrations, ionic transport shifts from single free charge carriers to clusters of salt nucleating, which has the primary function of scaling down the conductivity by forming neutral clusters. To account

for aggregate effect, Grossman et al. reformulated the Nernst-Einstein equation with the assumption that clusters do not interact with each other:[34]

$$\sigma_{cNE} = \frac{e^2}{Vk_BT}\sum_{i=0}^{N_+}\sum_{j=0}^{N_-} z^2{}_{ij}\alpha_{ij}D_{ij} \tag{3}$$

where the fundamental charge carrier are no longer single free ions but ionic clusters of different charge numbers $z_{ij} = iz_+ + jz_-$. α_{ij} is the matrix element that defines the population of the cluster consisted of i cations and j anions, which is averaged over ensembles and long simulation time. D_{ij} is the diffusion coefficient for each type of cluster, written in matrix form. Cation(s) and anion(s) are defined to belong to the same cluster if the cation is within the cutoff distance of one or more of the anions. It is worth noting that neutral cluster with $z_{ij} = 0$ does not contribute to the total conductivity although it also diffuses. This is the first time that the cluster Nernst-Einstein (cNE) is applied to polymer-in-salt system other than PEO or PEO-based variants.[61]

Molecular dynamics ion hopping analysis. The ion hopping analysis is characterized by tracking the coordination environment change of one single ion. Time-dependent trajectory of cation coordination is traced based on a distance criterion (i.e., an atom contributes to the coordination of a cation when its distance to the cation is less than the coordination cutoff). Specifically, the coordination from the most electronegative nitrogen atoms of the polymer chains and the oxygen atoms of the anions is tracked over the simulation time. The consecutive indices corresponds to consecutive coordination from the same chain or anion, while the switch between two different consecutive line indicates a cation jump among chains.

Acknowledgement

The authors thank the support from Defense Advanced Research Project Agency Young Faculty Award (DARPA YFA; HR00112010004). This research made use of the Cornell Center for Materials Research Shared Facilities which are supported through the NSF MRSEC

program (DMR-1719875). This work is performed in part at the Cornell NanoScale Facility, a member of the National Nanotechnology Coordinated Infrastructure (NNCI), which is supported by the National Science Foundation (Grant NNCI-2025233). The authors acknowledge Ivan Keresztes for helping perform PFG SE NMR.

Supporting Information Available

Experimental methods and characterization data are available:

References

(1) Zhu, J.; Zhang, Z.; Zhao, S.; Westover, A. S.; Belharouak, I.; Cao, P.-F. Single-ion conducting polymer electrolytes for solid-state lithium–metal batteries: design, performance, and challenges. *Advanced Energy Materials* **2021**, *11*, 2003836.

(2) Wang, J.; Gao, D.; Lee, P. S. Recent progress in artificial muscles for interactive soft robotics. *Advanced Materials* **2021**, *33*, 2003088.

(3) Ma, S.; Zhang, Y.; Liang, Y.; Ren, L.; Tian, W.; Ren, L. High-performance ionic-polymer–metal composite: toward large-deformation fast-response artificial muscles. *Advanced Functional Materials* **2020**, *30*, 1908508.

(4) Xiao, K.; Wan, C.; Jiang, L.; Chen, X.; Antonietti, M. Bioinspired ionic sensory systems: the successor of electronics. *Advanced Materials* **2020**, *32*, 2000218.

(5) Tepermeister, M.; Bosnjak, N.; Dai, J.; Zhang, X.; Kielar, S. M.; Wang, Z.; Tian, Z.; Suntivich, J.; Silberstein, M. N. Soft Ionics: Governing Physics and State of Technologies. *Frontiers in Physics* **2022**, 453.

(6) Armand, M. Polymers with ionic conductivity. *Advanced Materials* **1990**, *2*, 278–286.

(7) Jiang, Y.; Yan, X.; Ma, Z.; Mei, P.; Xiao, W.; You, Q.; Zhang, Y. Development of the PEO based solid polymer electrolytes for all-solid state lithium ion batteries. *Polymers* **2018**, *10*, 1237.

(8) Ohno, H.; Yoshizawa, M.; Ogihara, W. Development of new class of ion conductive polymers based on ionic liquids. *Electrochimica Acta* **2004**, *50*, 255–261.

(9) Qian, W.; Texter, J.; Yan, F. Frontiers in poly (ionic liquid) s: syntheses and applications. *Chemical Society Reviews* **2017**, *46*, 1124–1159.

(10) Bhandari, B.; Lee, G.-Y.; Ahn, S.-H. A review on IPMC material as actuators and sensors: fabrications, characteristics and applications. *International journal of precision engineering and manufacturing* **2012**, *13*, 141–163.

(11) Schauser, N. S.; Seshadri, R.; Segalman, R. A. Multivalent ion conduction in solid polymer systems. *Molecular Systems Design & Engineering* **2019**, *4*, 263–279.

(12) Shin, J.-H.; Henderson, W. A.; Passerini, S. Ionic liquids to the rescue? Overcoming the ionic conductivity limitations of polymer electrolytes. *Electrochemistry Communications* **2003**, *5*, 1016–1020.

(13) Imbrogno, J.; Maruyama, K.; Rivers, F.; Baltzegar, J. R.; Zhang, Z.; Meyer, P. W.; Ganesan, V.; Aoshima, S.; Lynd, N. A. Relationship between Ionic Conductivity, Glass Transition Temperature, and Dielectric Constant in Poly (vinyl ether) Lithium Electrolytes. *ACS Macro Letters* **2021**, *10*, 1002–1007.

(14) Shen, K.-H.; Hall, L. M. Effects of ion size and dielectric constant on ion transport and transference number in polymer electrolytes. *Macromolecules* **2020**, *53*, 10086–10096.

(15) Wojtecki, R. J.; Meador, M. A.; Rowan, S. J. Using the dynamic bond to access macroscopically responsive structurally dynamic polymers. *Nature materials* **2011**, *10*, 14–27.

(16) Grindy, S. C.; Learsch, R.; Mozhdehi, D.; Cheng, J.; Barrett, D. G.; Guan, Z.; Messersmith, P. B.; Holten-Andersen, N. Control of hierarchical polymer mechanics with bioinspired metal-coordination dynamics. *Nature materials* **2015**, *14*, 1210–1216.

(17) Li, C.-H.; Zuo, J.-L. Self-healing polymers based on coordination bonds. *Advanced Materials* **2020**, *32*, 1903762.

(18) Khare, E.; Holten-Andersen, N.; Buehler, M. J. Transition-metal coordinate bonds for bioinspired macromolecules with tunable mechanical properties. *Nature Reviews Materials* **2021**, *6*, 421–436.

(19) Zhang, X.; Vidavsky, Y.; Aharonovich, S.; Yang, S. J.; Buche, M. R.; Diesendruck, C. E.; Silberstein, M. N. Bridging experiments and theory: isolating the effects of metal–ligand interactions on viscoelasticity of reversible polymer networks. *Soft Matter* **2020**, *16*, 8591–8601.

(20) Zhang, X.; Crisci, R.; Finlay, J. A.; Cai, H.; Clare, A. S.; Chen, Z.; Silberstein, M. N. Enabling Tunable Water-Responsive Surface Adaptation of PDMS via Metal–Ligand Coordinated Dynamic Networks. *Advanced Materials Interfaces* **2022**, *9*, 2200430.

(21) Wang, H.-N.; Meng, X.; Dong, L.-Z.; Chen, Y.; Li, S.-L.; Lan, Y.-Q. Coordination polymer-based conductive materials: ionic conductivity vs. electronic conductivity. *Journal of Materials Chemistry A* **2019**, *7*, 24059–24091.

(22) Sanoja, G. E.; Schauser, N. S.; Bartels, J. M.; Evans, C. M.; Helgeson, M. E.; Seshadri, R.; Segalman, R. A. Ion transport in dynamic polymer networks based on metal–ligand coordination: effect of cross-linker concentration. *Macromolecules* **2018**, *51*, 2017–2026.

(23) Schauser, N. S.; Sanoja, G. E.; Bartels, J. M.; Jain, S. K.; Hu, J. G.; Han, S.; Walker, L. M.; Helgeson, M. E.; Seshadri, R.; Segalman, R. A. Decoupling bulk me-

chanics and mono-and multivalent ion transport in polymers based on metal–ligand coordination. *Chemistry of Materials* **2018**, *30*, 5759–5769.

(24) Schauser, N. S.; Grzetic, D. J.; Tabassum, T.; Kliegle, G. A.; Le, M. L.; Susca, E. M.; Antoine, S.; Keller, T. J.; Delaney, K. T.; Han, S., et al. The role of backbone polarity on aggregation and conduction of ions in polymer electrolytes. *Journal of the American Chemical Society* **2020**, *142*, 7055–7065.

(25) Anderson, E. B.; Long, T. E. Imidazole-and imidazolium-containing polymers for biology and material science applications. *Polymer* **2010**, *51*, 2447–2454.

(26) Nikolaev, A.; Richardson, P. M.; Xie, S.; Canzian Llanes, L.; Jones, S. D.; Nordness, O.; Wang, H.; Bazan, G. C.; Segalman, R. A.; Clément, R. J., et al. Role of Electron-Deficient Imidazoles in Ion Transport and Conductivity in Solid-State Polymer Electrolytes. *Macromolecules* **2022**, *55*, 971–977.

(27) Zhou, W.; Wang, Z.; Pu, Y.; Li, Y.; Xin, S.; Li, X.; Chen, J.; Goodenough, J. B. Double-layer polymer electrolyte for high-voltage all-solid-state rechargeable batteries. *Advanced Materials* **2019**, *31*, 1805574.

(28) Lu, G.; Qiu, H.; Du, X.; Sonigara, K. K.; Wang, J.; Zhang, Y.; Chen, Z.; Chen, L.; Ren, Y.; Zhao, Z., et al. Heteroleptic Coordination Polymer Electrolytes Initiated by Lewis-Acidic Eutectics for Solid Zinc–Metal Batteries. *Chemistry of Materials* **2022**, *34*, 8975–8986.

(29) Dünweg, B.; Kremer, K. Molecular dynamics simulation of a polymer chain in solution. *The Journal of chemical physics* **1993**, *99*, 6983–6997.

(30) Shen, K.-H.; Fan, M.; Hall, L. M. Molecular dynamics simulations of ion-containing polymers using generic coarse-grained models. *Macromolecules* **2021**, *54*, 2031–2052.

(31) Boden, N.; Leng, S.; Ward, I. Ionic conductivity and diffusivity in polyethylene oxide/electrolyte solutions as models for polymer electrolytes. *Solid State Ionics* **1991**, *45*, 261–270.

(32) Molinari, N.; Mailoa, J. P.; Kozinsky, B. Effect of salt concentration on ion clustering and transport in polymer solid electrolytes: a molecular dynamics study of peo–litfsi. *Chemistry of Materials* **2018**, *30*, 6298–6306.

(33) Wheeler, D. R.; Newman, J. Molecular dynamics simulations of multicomponent diffusion. 1. Equilibrium method. *The Journal of Physical Chemistry B* **2004**, *108*, 18353–18361.

(34) France-Lanord, A.; Grossman, J. C. Correlations from ion pairing and the Nernst-Einstein equation. *Physical review letters* **2019**, *122*, 136001.

(35) Gupta, N. S.; Lee, K.-S.; Labouriau, A. Tuning Thermal and Mechanical Properties of Polydimethylsiloxane with Carbon Fibers. *Polymers* **2021**, *13*, 1141.

(36) Bresser, D.; Lyonnard, S.; Iojoiu, C.; Picard, L.; Passerini, S. Decoupling segmental relaxation and ionic conductivity for lithium-ion polymer electrolytes. *Molecular Systems Design & Engineering* **2019**, *4*, 779–792.

(37) Companik, J.; Bidstrup, S. The viscosity and ion conductivity of polydimethylsiloxane systems: 2. Ion concentration effects. *Polymer* **1994**, *35*, 4834–4841.

(38) Brandrup, J.; Immergut, E. H.; Grulke, E. A.; Abe, A.; Bloch, D. R. *Polymer handbook*; Wiley New York, 1999; Vol. 89.

(39) Fong, K. D.; Self, J.; McCloskey, B. D.; Persson, K. A. Ion correlations and their impact on transport in polymer-based electrolytes. *Macromolecules* **2021**, *54*, 2575–2591.

(40) Qi, D.; Zhang, K.; Tian, G.; Jiang, B.; Huang, Y. Stretchable electronics based on PDMS substrates. *Advanced Materials* **2021**, *33*, 2003155.

(41) Pignanelli, J.; Qian, Z.; Gu, X.; Ahamed, M. J.; Rondeau-Gagné, S. Modulating the thermomechanical properties and self-healing efficiency of siloxane-based soft polymers through metal–ligand coordination. *New Journal of Chemistry* **2020**, *44*, 8977–8985.

(42) Pignanelli, J.; Billet, B.; Straeten, M.; Prado, M.; Schlingman, K.; Ahamed, M. J.; Rondeau-Gagné, S. Imine and metal–ligand dynamic bonds in soft polymers for autonomous self-healing capacitive-based pressure sensors. *Soft Matter* **2019**, *15*, 7654–7662.

(43) Yuan, K.; Bian, H.; Shen, Y.; Jiang, B.; Li, J.; Zhang, Y.; Chen, H.; Zheng, J. Coordination number of Li+ in nonaqueous electrolyte solutions determined by molecular rotational measurements. *The Journal of Physical Chemistry B* **2014**, *118*, 3689–3695.

(44) Ueno, N.; Wakabayashi, T.; Morisawa, Y. Determining the coordination number of Li+ and glyme or poly (ethylene glycol) in solution using attenuated total reflectance-far ultraviolet spectroscopy. *Analytical Sciences* **2019**, 19C011.

(45) Jun, M.-S.; Choi, Y.-W.; Kim, J.-D. Solvent casting effects of sulfonated poly (ether ether ketone) for Polymer electrolyte membrane fuel cell. *Journal of Membrane Science* **2012**, *396*, 32–37.

(46) Bodas, D.; Khan-Malek, C. Formation of more stable hydrophilic surfaces of PDMS by plasma and chemical treatments. *Microelectronic engineering* **2006**, *83*, 1277–1279.

(47) Smith, G.; Chen, R.; Mapolie, S. The synthesis and catalytic activity of a first-generation poly (propylene imine) pyridylimine palladium metallodendrimer. *Journal of Organometallic Chemistry* **2003**, *673*, 111–115.

(48) Johnston, D. H.; Shriver, D. F. Vibrational study of the trifluoromethanesulfonate anion: unambiguous assignment of the asymmetric stretching modes. *Inorganic Chemistry* **1993**, *32*, 1045–1047.

(49) Plimpton, S. Fast parallel algorithms for short-range molecular dynamics. *Journal of computational physics* **1995**, *117*, 1–19.

(50) Sun, H. Force field for computation of conformational energies, structures, and vibrational frequencies of aromatic polyesters. *Journal of Computational Chemistry* **1994**, *15*, 752–768.

(51) Olsher, U.; Izatt, R. M.; Bradshaw, J. S.; Dalley, N. K. Coordination chemistry of lithium ion: a crystal and molecular structure review. *Chemical reviews* **1991**, *91*, 137–164.

(52) Humphrey, W.; Dalke, A.; Schulten, K. VMD: visual molecular dynamics. *Journal of molecular graphics* **1996**, *14*, 33–38.

(53) Eisenberg, A. Clustering of ions in organic polymers. A theoretical approach. *Macromolecules* **1970**, *3*, 147–154.

(54) Borodin, O.; Smith, G. D. Mechanism of ion transport in amorphous poly (ethylene oxide)/LiTFSI from molecular dynamics simulations. *Macromolecules* **2006**, *39*, 1620–1629.

(55) Rao, Y.-L.; Feig, V.; Gu, X.; Nathan Wang, G.-J.; Bao, Z. The effects of counter anions on the dynamic mechanical response in polymer networks crosslinked by metal–ligand coordination. *Journal of Polymer Science Part A: Polymer Chemistry* **2017**, *55*, 3110–3116.

(56) Chu, T.; Belding, L.; van der Est, A.; Dudding, T.; Korobkov, I.; Nikonov, G. I. A Coordination Compound of Ge0 Stabilized by a Diiminopyridine Ligand. *Angewandte Chemie International Edition* **2014**, *53*, 2711–2715.

(57) Kim, K.; Kuhn, L.; Alabugin, I. V.; Hallinan Jr, D. T. Lithium salt dissociation in

diblock copolymer electrolyte using fourier transform infrared spectroscopy. *Frontiers in Energy Research* **2020**, *8*, 569442.

(58) Cheng, Y.; Yang, J.; Hung, J.-H.; Patra, T. K.; Simmons, D. S. Design rules for highly conductive polymeric ionic liquids from molecular dynamics simulations. *Macromolecules* **2018**, *51*, 6630–6644.

(59) Bocharova, V.; Sokolov, A. P. Perspectives for polymer electrolytes: a view from fundamentals of ionic conductivity. *Macromolecules* **2020**, *53*, 4141–4157.

(60) Fujie, K.; Ikeda, R.; Otsubo, K.; Yamada, T.; Kitagawa, H. Lithium ion diffusion in a metal–organic framework mediated by an ionic liquid. *Chemistry of Materials* **2015**, *27*, 7355–7361.

(61) France-Lanord, A.; Wang, Y.; Xie, T.; Johnson, J. A.; Shao-Horn, Y.; Grossman, J. C. Effect of chemical variations in the structure of poly (ethylene oxide)-based polymers on lithium transport in concentrated electrolytes. *Chemistry of Materials* **2019**, *32*, 121–126.

(62) Mindemark, J.; Lacey, M. J.; Bowden, T.; Brandell, D. Beyond PEO—Alternative host materials for Li+-conducting solid polymer electrolytes. *Progress in Polymer Science* **2018**, *81*, 114–143.

(63) Gouverneur, M.; Schmidt, F.; Schönhoff, M. Negative effective Li transference numbers in Li salt/ionic liquid mixtures: does Li drift in the "Wrong" direction? *Physical Chemistry Chemical Physics* **2018**, *20*, 7470–7478.

(64) Hu, Z.; Kerton, F. M. Room temperature aerobic oxidation of alcohols using CuBr2 with TEMPO and a tetradentate polymer based pyridyl-imine ligand. *Applied Catalysis A: General* **2012**, *413*, 332–339.

(65) Zuidema, J. M.; Rivet, C. J.; Gilbert, R. J.; Morrison, F. A. A protocol for rheological characterization of hydrogels for tissue engineering strategies. *Journal of Biomedical Materials Research Part B: Applied Biomaterials* **2014**, *102*, 1063–1073.

(66) Rubinstein, M.; Colby, R. H., et al. *Polymer physics*; Oxford university press New York, 2003; Vol. 23.

(67) Ratner, M. A.; Shriver, D. F. Ion transport in solvent-free polymers. *Chemical reviews* **1988**, *88*, 109–124.

(68) Schlenoff, J. B.; Akkaoui, K. Dissecting dynamics near the glass transition using polyelectrolyte complexes. *Macromolecules* **2021**, *54*, 3413–3422.

(69) Chen, H.; Choi, J.-H.; Salas-de la Cruz, D.; Winey, K. I.; Elabd, Y. A. Polymerized ionic liquids: the effect of random copolymer composition on ion conduction. *Macromolecules* **2009**, *42*, 4809–4816.

(70) Klein, R. J.; Zhang, S.; Dou, S.; Jones, B. H.; Colby, R. H.; Runt, J. Modeling electrode polarization in dielectric spectroscopy: Ion mobility and mobile ion concentration of single-ion polymer electrolytes. *The Journal of chemical physics* **2006**, *124*, 144903.

(71) Stacy, E. W.; Gainaru, C. P.; Gobet, M.; Wojnarowska, Z.; Bocharova, V.; Greenbaum, S. G.; Sokolov, A. P. Fundamental limitations of ionic conductivity in polymerized ionic liquids. *Macromolecules* **2018**, *51*, 8637–8645.

(72) Wang, J.; Hou, T. Application of molecular dynamics simulations in molecular property prediction II: Diffusion coefficient. *Journal of computational chemistry* **2011**, *32*, 3505–3519.

(73) in't Veld, P. J.; Rutledge, G. C. Temperature-dependent elasticity of a semicrystalline interphase composed of freely rotating chains. *Macromolecules* **2003**, *36*, 7358–7365.

(74) Leontyev, I.; Stuchebrukhov, A. Accounting for electronic polarization in non-polarizable force fields. *Physical Chemistry Chemical Physics* **2011**, *13*, 2613–2626.

(75) Fick, A. Ueber diffusion. *Annalen der Physik* **1855**, *170*, 59–86.